Free-Surface Time-Series Generation for Wave Energy Applications

Alexis Mérigaud and John V. Ringwood, *Senior Member, IEEE*

***Abstract*—Finite-length, numerical simulations of Gaussian seas are widely used in the wave energy sector. The most common method consists of adding up harmonic sinusoidal components, with random phases and deterministic amplitudes derived from the target wave spectrum [deterministic amplitude scheme (DAS)]. In another approach, the component amplitudes are chosen randomly with a variance depending on the spectrum [random amplitude scheme (RAS)]. It is now generally accepted that only the latter method reproduces the true statistical properties of a Gaussian sea. Compared to previous works, this study clarifies the exact nature of the "statistical properties" that should be represented in the simulation process. Further analysis is carried out to address unanswered questions highlighted in the existing literature, especially with respect to the statistical relationships between discrete successive simulation points, and the probability law governing the average power estimator of a wave energy converter (WEC) simulated with the generated wave time series. It is shown that RAS exactly reflects how the WEC performance, considered over a finite duration, varies with respect to its long-term average, whereas DAS has the advantage of providing accurate estimates of the long-term average values using fewer, or shorter, simulations; in particular, it is demonstrated that only one simulation is sufficient when the WEC model is linear. Furthermore, it is shown why alternative methods, based on nonharmonic superposition of sinusoids, are not recommended. The effects of the simulation method (RAS or DAS) upon the statistics of individual oscillations in the time domain are also explored experimentally. Finally, a table is provided that gives recommendations, depending on the objective of the simulations.**

***Index Terms*—Average power estimation, Gaussian sea, numerical simulation, time-domain statistics, wave energy converter (WEC), wave spectrum.**

I. Introduction

THE numerical generation of ocean free-surface elevation time series is important across many marine technology fields. In particular, discrete-time, finite-duration simulations of Gaussian seas with appropriate statistical properties are useful in various offshore engineering applications.

In the field of wave energy, time-series generation is especially important for wave energy converter (WEC) design and performance assessment—including control design—and for wave energy forecasting. The common practice consists of adding a finite number of sinusoidal, harmonic Fourier components with random phases and deterministic amplitudes. In the following, this method will be referred to as deterministic amplitude scheme (DAS). For a target spectral density function (SDF) denoted $S(f)$, and a finite realization of length $T = N\Delta t$, the discrete sequence of simulated free surface elevation η_{t_i} with $t_i = i\Delta t, i = 1 \dots N$, can be written as follows:

$$\eta_{t_i} = \sum_{k=1}^{M/2} A_k \cos(2\pi f_k t_i + \phi_k) \tag{1}$$

where $M/2$ is the number of discrete frequency components (typically, $M = N$); $f_k = k\Delta f, k = 1, \dots, M/2$ and $\Delta f = 1/M\Delta t$; $A_k = \sqrt{2S(f_k)\Delta f}$; and ϕ_k is randomly chosen following a uniform distribution in $[0; 2\pi]$.

DAS can be computed using fast Fourier transform (FFT) and, thus, offers the advantage of computational efficiency and simplicity; furthermore, it does not seem to introduce any bias when used to estimate some specific average time-domain quantities [1]. However, as first pointed out in [2], DAS does not reproduce the statistical properties of a true Gaussian sea. For example, wave group statistics may not be accurately reproduced. Besides, DAS exactly preserves the spectral moments of the SDF at each realization [1], which practically means that the spectral moment estimators evaluated in the time domain take the very same value at each realization of the simulated process. In contrast, when taking discrete measurements of a true Gaussian process, the estimators based on a finite number of values would present some variability, only converging toward the actual spectral moment values as N tends to infinity with Δt constant. Therefore, running simulations with DAS cannot deliver proper statistical information such as, for example, the dispersion of WEC performance around its average.

A number of other methods for free-surface time-series generation have been discussed in the literature and can be broadly classified into other wave superposition methods and white noise filtering. Among the former, the random amplitude scheme (RAS) is as simple and computationally efficient as DAS and allows for reproducing more realistically the properties of a Gaussian process [1], [2].

The discrete sequence generated through RAS can be written as follows:

$$\eta_{t_i} = \sum_{k=1}^{M/2} a_k \cos(2\pi f_k t_i) + b_k \sin(2\pi f_k t_i) \tag{2}$$

Manuscript received July 5, 2016; revised January 11, 2017; accepted March 31, 2017. Date of publication April 26, 2017; date of current version January 11, 2018. This work was supported by Science Foundation Ireland under Grant 12/RC/2302 for the Marine Renewable Ireland Centre. *(Corresponding author: Alexis Mérigaud.)*

Associate Editor: B. Buckham.

The authors are with the Department of Electronic Engineering, Centre for Ocean Energy Research,Maynooth University, Maynooth, co. Kildare, Ireland (e-mail: alexis.merigaud.2015@mumail.ie; john.ringwood@nuim.ie).

Digital Object Identifier 10.1109/JOE.2017.2691199

where, this time, a_k and b_k are chosen as independent, normally distributed random variables with zero mean and variance $S(f_k)\Delta f$. The RAS discrete sequence can also be formulated as

$$\eta_{t_i} = \sum_{k=1}^{M/2} A_k \cos(2\pi f_k t_i + \phi_k) \tag{3}$$

where ϕ_k is randomly chosen following a uniform distribution in $[0; 2\pi]$; and A_k follows a Rayleigh distribution with variance $2S(f_k)\Delta f$.

The two formulations are strictly equivalent—in fact, $A_k^2 = a_k^2 + b_k^2$.

Following the work presented in [1] and [2] and observing that, in spite of recommended practice [3], most researchers and engineers still mainly use DAS in an uninformed way, this study advocates again the use of RAS as soon as probabilistic information is needed on finite-length simulations—uncertainty on performance, extreme values, etc.—and highlights the precautions that should be taken when using DAS. A number of theoretical points that were not clarified in previous works [1], [2] are also explicitly developed. The ambition of this paper is to offer a clear and informed alternative between DAS and RAS, the former being suitable in some specific cases when only an average time-domain value is needed, while the latter perfectly reproduces the properties of the actual Gaussian sea process and thus provides the right tool for any probabilistic analysis of finite-length simulations.

The structure of this paper is as follows. Section II formulates the simulation problem in a clear and explicit way. It is shown in Section III that RAS enables us to reproduce almost perfectly the desired statistical properties of a Gaussian sea such as defined in Section II. Section IV explores the statistical properties of two important time-domain estimators, namely, the zeroth-order spectral moment estimator and the average WEC power estimator, showing in particular the impact of the chosen simulation method (DAS or RAS) on the estimator statistical properties. It is shown, in Section V, why using alternative methods, based on nonharmonic sinusoid superposition, is not recommended. In Section VI, numerical simulations confirm and illustrate the results of Section IV, and present a few more experimental results obtained with other time-domain statistics. Theoretical and experimental results and their practical implications are discussed in Section VII. Finally, Section VIII provides conclusions as well as recommendations to engineers and researchers who need to simulate Gaussian free-surface elevation time series.

II. Problem Formulation

A. Ocean Wave Elevation as a Stationary Gaussian Process

Ocean waves can be modeled as a stationary, zero-mean Gaussian process in most conditions, i.e., as long as water depth is sufficient and the wave condition is not too extreme. For more justification and details on the range of validity of the Gaussian sea description, see [4].

A Gaussian process is a specific category of stochastic processes, in which every finite collection of measurements taken at different points in time follows a multivariate normal distribution. In particular, any single measurement taken at a given point in time is a normally distributed random variable.

Furthermore, when the duration considered is small compared to the typical rate at which the sea condition evolves in time, the stochastic process of sea surface elevation can be considered as being stationary. For a stochastic process in general, stationarity means that all statistical properties of the process are invariant by translation in time. For a Gaussian process, the stationarity condition reduces to time invariance of the first- and second-order statistical moments, which is called weak stationarity [4]. Finally, the sea surface Gaussian process is also considered to be ergodic [4], which means that time averages of the process are equal to ensemble averages.

Such a stationary ergodic Gaussian process is entirely characterized by its mean ($\bar{\eta} = 0$) and its autocovariance function (ACVF) $R_{\eta\eta}$ defined as

$$R_{\eta\eta}(\tau) = \lim_{T\to\infty} \frac{1}{2T} \int_{-T}^{T} \eta(t)\eta(t+\tau)dt. \tag{4}$$

The fact that $R_{\eta\eta}$ only depends on τ stems from the process stationarity. Furthermore, $R_{\eta\eta}(\tau)$ is an even function that reaches its maximum in $\tau = 0$, with $R_{\eta\eta}(0)$ being equal to the variance of the process.

Thanks to the ergodicity property of the process, $R_{\eta\eta}$ can also be defined as

$$R_{\eta\eta}(\tau) = \mathbb{E}[\eta(t)\eta(t+\tau)]. \tag{5}$$

Besides, let us define the SDF $S_{\eta\eta}(f)$ of the process as

$$S_{\eta\eta}(f) = \lim_{T\to\infty} \frac{1}{T} |H_T(f)|^2 \tag{6}$$

where $H_T(f) = \int_{-T}^{T} \eta(t) \mathrm{e}^{-i2\pi ft} dt$.

The ACVF and the SDF of the weakly stationary sea surface elevation process are Fourier transforms of each other, according to the Wiener–Khintchine theorem

$$S_{\eta\eta}(f) = 2\int_{-\infty}^{\infty} R_{\eta\eta}(\tau) \mathrm{e}^{-i2\pi f\tau} d\tau \tag{7}$$

and

$$R_{\eta\eta}(\tau) = \frac{1}{2}\int_{-\infty}^{\infty} S_{\eta\eta}(f) \mathrm{e}^{i2\pi f\tau} df. \tag{8}$$

As a consequence, the statistical properties of the stationary, zero-mean Gaussian wave elevation process are entirely described by its ACVF, or equivalently by its SDF.

In practice, the latter is more often available. Indeed, the wave spectrum can be easily estimated by means of Fourier transforms of a recorded wave elevation signal. Furthermore, the wave SDF is very informative since it exhibits the frequency content of the wave, which is useful to study the frequency response of ships or offshore structures. Finally, meteorological models that include ocean wave conditions also describe sea states by means of the wave SDF.

However, as pointed out in [4], the mathematical tools for stochastic analysis of Gaussian waves strongly rely on the fact that SDF and ACVF are two equivalent ways of representing the statistical properties of the sea surface as a stochastic process.

B. Discrete-Time Simulation

In numerical simulations, the very notion of a continuous-time process has no actual meaning because whatever the level of temporal resolution, discrete values are generated. While the focus of this paper is finite-length, discrete-time simulations of wave elevation, so far in this section only a continuous-time stochastic process has been considered. Then, how should the fidelity of the time-series generation method to the underlying process be evaluated?

1) Measurements of a Gaussian Process—A Conceptual Experiment: To answer this question, let us consider a conceptual experiment where N discrete measurements of the (actual) sea surface elevation are taken at the very same location, at regular time interval Δt between two consecutive measurements. It is assumed in Section II-A that the sea is a stationary, ergodic Gaussian process. Let us consider the probability law jointly followed by the N measurement values, indexed by $i \in 1, \ldots, N$ so that $t_i = i\Delta t$. From the definition of a Gaussian process, the joint probability of the N measurements follows a multivariate normal distribution of dimension N. This N-dimensional Gaussian is characterized by its mean ($0_{\mathbb{R}^N}$) and its variance-covariance matrix $\Sigma_{\eta\eta} \in \mathbb{R}^{N\times N}$

$$\begin{aligned} \forall i,j \in \{1,\ldots,N\}, \Sigma_{\eta\eta,ij} &= \mathbb{E}[\eta(t_i)\eta(t_j)] \\ &= \mathbb{E}[\eta(i\Delta t)\eta(j\Delta t)] \\ &= R_{\eta\eta}((j-i)\Delta t). \end{aligned} \tag{9}$$

The variance-covariance matrix of the measured process $\Sigma_{\eta\eta}$ is a symmetric, positive definite Toeplitz matrix. Its diagonal elements are all equal to the variance of the process, i.e.,

$$\forall i \in \{1,\ldots,N\}, \Sigma_{\eta\eta,ii} = \mathbb{E}[\eta(t_i)^2] = R_{\eta\eta}(0) = \int_0^\infty S_{\eta\eta}(f)df. \tag{10}$$

By denoting $r_i = R_{\eta\eta}(i\Delta t)$ for all $i \in \{0,\ldots,N-1\}$, and recalling that $R_{\eta\eta}$ is even, then each line of $\Sigma_{\eta\eta}$ is a discretized, time-shifted version of the ACVF, i.e.,

$$\Sigma_{\eta\eta} = \begin{pmatrix} r_0 & r_1 & r_2 & \cdots & r_{N-1} \\ r_1 & r_0 & r_1 & \cdots & r_{N-2} \\ \vdots & & \ddots & & \vdots \\ \vdots & & & \ddots & \vdots \\ r_{N-1} & r_{N-2} & \cdots & r_1 & r_0 \end{pmatrix}. \tag{11}$$

2) Back to the Simulation Problem: For the simulation method to be correct, the experiment, consisting of *simulating* N consecutive values of free-surface elevation, should be equivalent to the conceptual experiment consisting of *measuring* N consecutive samples of the "true" Gaussian process.

Finally, the simulation problem can be stated in a rigorous way. A finite, discrete-time simulation method accurately reflects an actual Gaussian sea with known ACVF provided that we have the following.

1) The simulated vector, denoted $y \in \mathbb{R}^N$, follows an N-dimensional, zero-mean Gaussian distribution. In particular, every single component of the vector must follow a zero-mean Gaussian law.
2) The variance-covariance matrix of the simulated vector Σ_{yy} is equal to, or at least a good approximation of $\Sigma_{\eta\eta} = (r_{|i-j|})_{i,j\in\{1,\ldots,N\}}$.

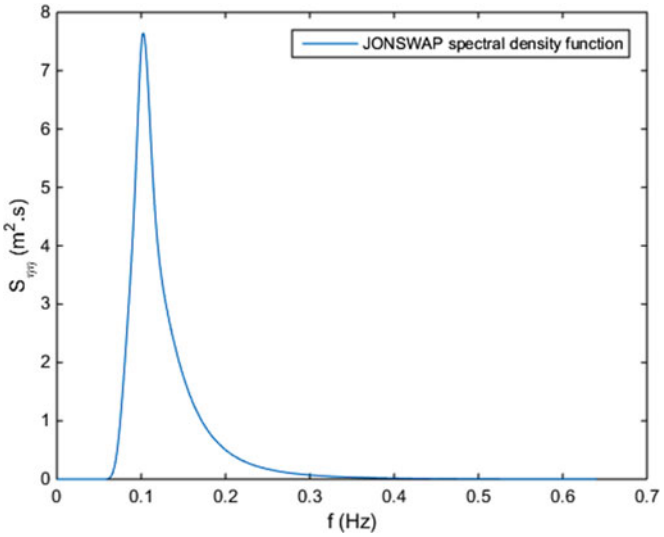

Fig. 1. SDF for a sea state with JONSWAP spectrum with $H_{m_0} = 2.45$ m, $T_p = 9.8$ s, and $\gamma = 1.7$.

While it was unclear, in previous works, what was exactly meant by the "statistical properties" that the simulated process should exhibit, the objectives are now explicitly formulated. Since a Gaussian vector is entirely characterized by its mean and variance-covariance matrix, no other property is needed in addition to the two conditions stated above. Section III shows why RAS meets such requirements.

III. Random Amplitude Scheme as a Suitable Gaussian Sea Simulation Tool

A. Preliminary Observations

Let us first have a look at the ACVF of a typical Gaussian sea. The sea state considered is described by a Joint North Sea Wave Project (JONSWAP[5]) spectrum pictured in Fig. 1. The ACVF corresponding to the same sea state is represented in Fig. 2, obtained through numerical integration of the Wiener–Khintchine relation of (8). Fig. 3 represents the discretized version of $R_{\eta\eta}$, for positive lags, and can then be seen as the first line of $\Sigma_{\eta\eta}$ as described in (11).

Three remarks are appropriate. First, the ACVF of typical wave spectra consists of damped oscillations fading out to zero after several tens of seconds. As far as the discrete ACVF is concerned, it means that it is possible to define an integer $K \in \mathbb{N}^{+*}$ such that $\forall i \geq K, r_i \approx 0$. Under this condition, the process to model is a stationary, K-correlated process, which means that it is possible to describe it as a stationary moving-average process of order K [6]. Second, inspired by Fig. 1, it can be considered that the frequency range of the available spectrum is high enough to include all the frequency content of interest; in other words, for all $f \geq (M/2)\Delta f$, $S_{\eta\eta}(f) = 0$. Finally, let us

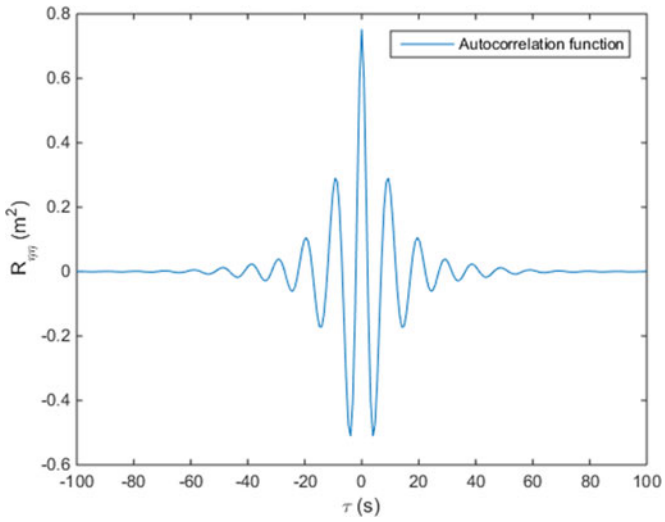

Fig. 2. Continous ACVF for the sea state represented in Fig. 1.

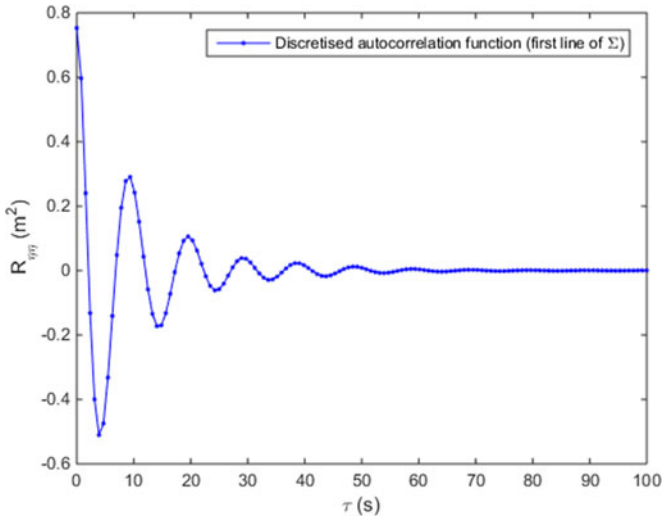

Fig. 3. Discrete ACVF for the sea state represented in Fig. 1, for positive lags.

recall that $S_{\eta\eta}(f)$ is an even function, although only the positive frequencies are usually shown.

B. Statistical Properties of the Random Amplitude Scheme Generated Signal

Let us now simulate N consecutive values of the free-surface elevation by applying RAS (2), based on the SDF $S_{\eta\eta}(f)$, for example, the one presented in Fig. 1. In the following, the vector of simulated values is denoted $y \in \mathbb{R}^N$.

For now, let us not make any assumption on the number of frequency components M so that possibly $M \neq N$. M is an even number, typically a power of 2. Furthermore, M and Δf are set in accordance with each other so as to cover the whole range of frequencies contained in $S_{\eta\eta}$, and the maximum frequency considered corresponds to the Nyquist frequency so that

$$\frac{M}{2}\Delta f = f_{\max} = \frac{1}{2\Delta t}. \tag{12}$$

Let ϵ be a vector of M independent identically distributed Gaussian random variables with zero mean and unit variance: $\forall i \in \{1,\dots,M\}, \epsilon_i \sim \mathcal{N}(0,1)$. The law of ϵ follows a multivariate Gaussian distribution with mean $0_{\mathbb{R}^M}$ and a variance-covariance matrix equal to the identity matrix $I_{\mathbb{R}^{M\times M}}$.

Then, let us define $A \in \mathbb{R}^{N\times M}$ by

$$A_{ij} = \begin{cases} \sqrt{S_{\eta\eta}(f_j)\Delta f}\cos(2\pi f_j t_i), & \text{for } j \in \left\{1,\dots,\frac{M}{2}\right\} \\ \sqrt{S_{\eta\eta}(f_j)\Delta f}\sin(2\pi f_j t_i), & \text{for } j \in \left\{\frac{M}{2}+1,\dots,M\right\}. \end{cases} \tag{13}$$

The simulated free-surface elevation y is generated with RAS as $y = A\epsilon$. y is then clearly a linear transformation of a Gaussian vector with zero mean; it is then also a Gaussian vector with zero mean, and its variance-covariance matrix is equal to $\Sigma_{yy} = AIA^T = AA^T$, where $(\cdot)^T$ denotes the transpose. A cumbersome but straightforward calculation shows that Σ_{yy} has the same structure as $\Sigma_{\eta\eta}$, i.e.,

$$\Sigma_{yy} = \begin{pmatrix} s_0 & s_1 & s_2 & \cdots & s_{N-1} \\ s_1 & s_0 & s_1 & \cdots & s_{N-2} \\ \vdots & & \ddots & & \vdots \\ \vdots & & & \ddots & \vdots \\ s_{N-1} & s_{N-2} & \cdots & s_1 & s_0 \end{pmatrix}. \tag{14}$$

More precisely, assuming $S_{\eta\eta}(f_0) = S_{\eta\eta}(0) = 0$, and since $S_{\eta\eta}(-f) = S_{\eta\eta}(f)$

$$\begin{aligned} \forall j \in \{0,\dots,N-1\}, s_j &= \sum_{k=1}^{\frac{M}{2}} S_{\eta\eta}(f_k)\Delta f \cos(2\pi f_k j\Delta t) \\ &= \frac{1}{2}\sum_{k=-\frac{M}{2}}^{\frac{M}{2}} S_{\eta\eta}(f_k)\mathrm{e}^{\mathrm{i}2\pi f_k j\Delta t}\Delta f. \end{aligned} \tag{15}$$

One recognizes in (15) a Riemann approximation of integral (8). When the frequency step Δf is refined, the approximation gets closer and closer to the target discretized ACVF. Since one considers a finite-duration time interval, and assuming that the spectrum $S_{\eta\eta}$ is a continuous function of f, the Riemann approximation converges, and for any desired degree of accuracy, it is possible to find a frequency step Δf so that for all lags within the simulation interval, the ACVF error is smaller than the chosen threshold. However [7], unlike the actual discrete ACVF sequence, $(s_j)_{j\in\mathbb{N}}$ is periodic with period M. Typically, with $N = M$, $(s_j)_{j=1,\dots,M}$ resembles a "folded" version of the target ACVF sequence, $(r_j)_{j=1,\dots,M}$ (see Fig. 4).

The ACVF of the signal being periodic is equivalent to the signal itself being periodic—and indeed, any signal generated through the superposition of harmonic sinusoids is periodic, with a period equal to the inverse of the fundamental frequency

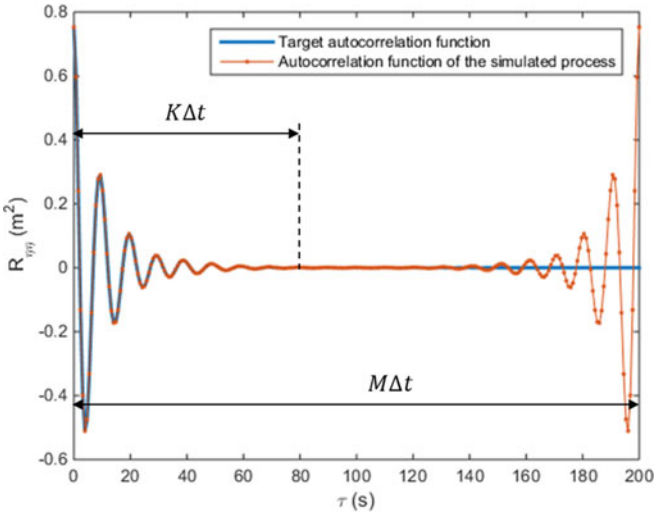

Fig. 4. Target and simulated ACVF for $M = N$, $\Delta f = 1/(N\Delta t)$, $\Delta t = 1/1.28 \approx 0.78$ s, and $T = N\Delta t = 200$ s.

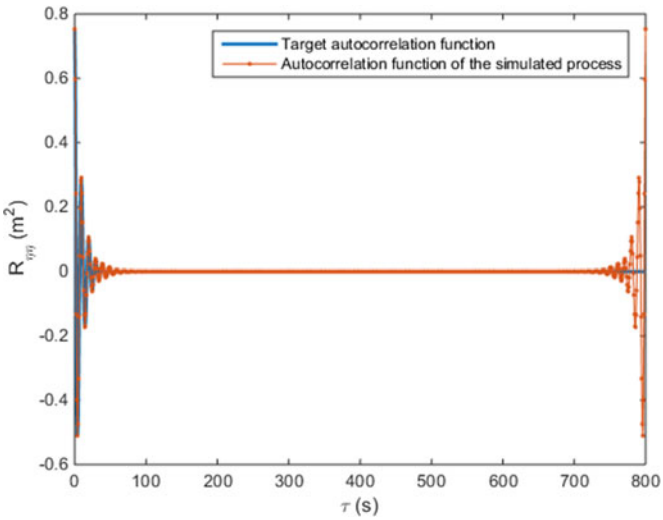

Fig. 5. Target and simulated ACVF for $M = N$, $\Delta f = 1/(N\Delta t)$, and $T = N\Delta t = 800$ s.

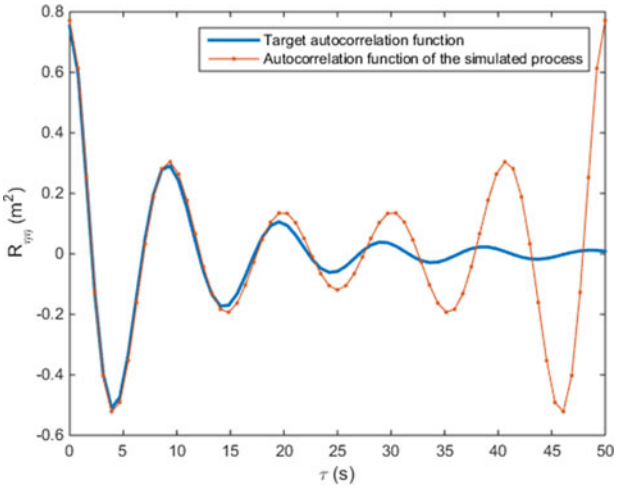

Fig. 6. Target and simulated ACVF for $M = N$, $\Delta f = 1/(N\Delta t)$, and $T = N\Delta t = 50$ s.

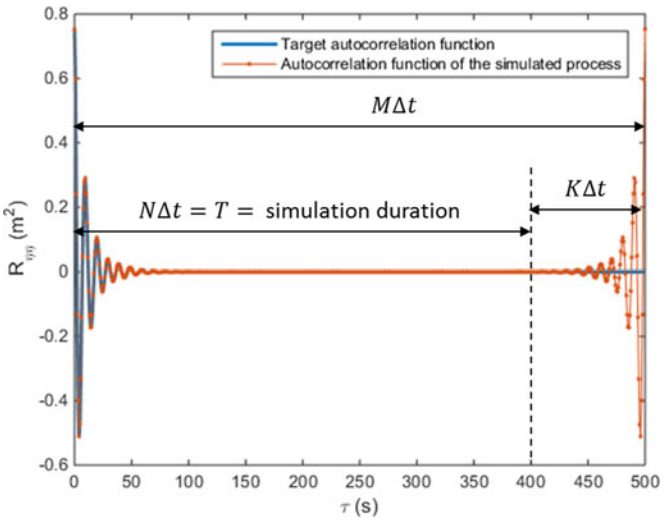

Fig. 7. Target and simulated ACVF for $\Delta f = 1/(M\Delta t)$, $M = N + K$, and $T = N\Delta t = 400$ s.

Δf. To avoid self-repetition of the signal within the simulation window, along with poor matching to the target statistical properties, a first condition for RAS to work well is to set $M \geq N$.

Setting $M = N$, one can observe in Fig. 4 that the discrete ACVF of the generated signal agrees well with the target one, except for the self-repetition issue for the lags close to N. As far as ocean waves are concerned, as mentioned earlier in Section III-A, it is possible to define K, such that the target discrete ACVF is considered to be zero for lags greater than K. As a consequence, the self-repetition issue only plays a role in the joint probabilistic properties of the first K and the last K generated samples (if $M = N$). Thus, it may not be significant if the simulation time is very long, such that $M \gg K$ (see Fig. 5). But in shorter signals, when M and K have the same order of magnitude, the statistical properties of the generated signal are significantly affected (see Fig. 6).

A simple way to circumvent the self-repetition issue is to choose M such that the period of the generated signal exceeds the simulation length by the correlation length of the signal; in other words, $M/(\Delta f) \geq (N + K)\Delta t$ (see Fig. 7).

In summary, the law of the random vector generated with RAS follows a multivariate, N-dimensional Gaussian distribution, and its variance-covariance matrix is an excellent approximation to $\Sigma_{\eta\eta}$ provided that $M \geq K + N$. The latter restriction can even be removed for long simulations.

C. Additional Remarks

1) Restriction on M: The restriction $M \geq N + K$ is important in theory; however, in practice, it may not be necessary, for two reasons.

1) By simply letting $M = N$, as stated in Section III-B, the undue autocorrelation is only significant for the first and last points of the simulation so that in long simulations the overall statistical properties of the simulated process are barely affected.

2) The wave elevation time series is more often used within a time-domain simulation of a dynamical system, taking the waves as an input. Typically, only the system steady state is considered so that the first part of the simulation is often discarded as corresponding to a transient time. Thus, if the transient time considered is longer than the autocorrelation length of the signal (i.e., there are more than K discarded samples), then the periodicity of the simulated signal is not an issue any more and one can simply let $M = N$.

Finally, in the case that M really has to be restricted to be greater than $N + K$, one may argue that the FFT then cannot be used, and thus, RAS loses the advantage of computational efficiency. But that would not be a relevant argument since, even when $M \geq N$, one can still generate y using FFT and simply discard the unnecessary samples.

2) Exact Method: Since the process considered can be seen as a moving average model of order K, it would also have been possible to apply the so-called exact frequency-domain method presented in [7], which would involve the following:

1) computing the discrete ACVF (r_i) at a very high degree of accuracy through numerical integration of (8);
2) computing (S_k), the DFT of (r_i);
3) simulating the signal using (2) but replacing $S_{\eta\eta}(f_k)$ with S_k.

Then, if $K \leq N \leq M/2$, the discrete ACVF of the generated signal is exactly equal to the true ACVF r_i obtained through numerical integration.

However, applying RAS with typical M values, the ACVF of the generated signal is already an excellent approximation to the target one (in Figs. 4, 5, 7, and 14 presented in this paper, the difference between both is invisible except for the last K samples), so that it is preferable to use RAS, which is directly based on the readily available SDF.

3) Subsets of the Generated Time Series: It should also be mentioned that if N samples of free surface elevation are generated through RAS and N' consecutive samples are chosen ($N' < N$) from the N initial samples, the joint probability distribution of the N' samples also follows a multivariate Gaussian law with the desired properties: It is equivalent to generate N' samples with RAS directly, or to generate $N > N'$ sample through RAS and choosing N' consecutive samples.

4) Law of the Time Series Generated With Deterministic Amplitude Scheme: In contrast to RAS, the vectors generated through DAS do not even follow a Gaussian law: Based on (1), the simplest way to see it is to note that the generated process is bounded by the sum of $A_k, k \in \{1, \ldots, M/2\}$.

In fact, DAS corresponds to a very specific subset of possible RAS realizations, in which for all k in $\{1, \ldots, M/2\}$, $a_k^2 + b_k^2 = 2S(f_k)\Delta f$. Then, some of the intersimulation variability is lost.

Even though the vector generated through DAS does not follow a multivariate Gaussian law, it is still possible to define its variance-covariance matrix. The same calculations as in Section III-B show that its variance-covariance matrix is exactly the same as with RAS. Then, it can be said that for DAS as for RAS, the intrasimulation signal variability is well represented, i.e., that the statistical correlation between the different simulated points is correct for the two simulation methods.

IV. m_0 and $\bar{P}_{\mathrm{PTO}}$ Estimators

This section presents practical implications of the theoretical results derived in Section III, in terms of common time-domain statistics. As in [1], two statistics are examined here as follows.

1) The estimator $\hat{m}_0$ for the zeroth order spectral moment of the signal (also equal to the signal variance).
2) The estimator $\hat{P}_{\mathrm{PTO}}$ of the average power production $\bar{P}_{\mathrm{PTO}}$ of a WEC moved by the simulated waves. m_0 is related to important characteristics of the sea state, such as:
   a) the average stored energy per unit horizontal surface E related to m_0 through $E = \rho g m_0$, where ρ denotes the seawater density and g the gravitational constant (see, for example, [8, ch. 4]);
   b) the significant wave height H_{m_0}, which is often used in wave energy calculations, is related to m_0 through a relationship that depends on the spectral bandwidth (see [4, ch. 3]).

Furthermore, it will be shown in Section IV-C that $\hat{P}_{\mathrm{PTO}}$ can be studied in the same way as $\hat{m}_0$, which, therefore, constitutes a useful preliminary.

The average power output is essential to assess WEC performance, thus understanding the statistical behavior of $\hat{P}_{\mathrm{PTO}}$ in finite-length simulations is crucial, for example, to determine how many simulations are necessary, or how long they should be, to obtain an accurate estimate of $\bar{P}_{\mathrm{PTO}}$. Furthermore, one may not only want to know the average power output $\bar{P}_{\mathrm{PTO}}$ of the WEC, but also how the WEC performance over a finite duration fluctuates around its average value.

A. m_0 Estimator for the Actual Gaussian Process

The zeroth-order spectral moment m_0 is equal to the wave signal variance

$$m_0 = \int_0^\infty S_{\eta\eta}(f)df = \mathbb{E}[\eta(t)\eta(t)] = R_{\eta\eta}(0). \tag{16}$$

Given N' regularly spaced sample points $\eta_n, n \in \{1, \ldots, N'\}$, the time-domain variance estimator is given by

$$\hat{m}_0 = \frac{1}{N'} \sum_{n=1}^{N'} \eta_n^2. \tag{17}$$

It can be shown that the variance of such an estimator is given as follows (see, for example, [9]):

$$\sigma^2_{\hat{m}_0} = \frac{2}{N'} \sum_{n=-N'}^{N'} \left(1 - \frac{|n|}{N'}\right) R^2_{\eta\eta}(n\Delta t). \tag{18}$$

Alternatively, instead of considering individual samples, m_0 can be estimated through an integral over $[0; T']$ with $T' = N'\Delta t$ so that

$$\hat{m}_0 = \frac{1}{T'} \int_0^{T'} \eta^2(t)dt. \tag{19}$$

Then, (18) becomes

$$\sigma^2_{\hat{m}_0} = \frac{2}{T'}\int_{-T'}^{T'}\left(1-\frac{|t|}{T'}\right)R^2_{\eta\eta}(t)dt. \tag{20}$$

The above expression is not straightforward to analyze for small T' (or N'); however, since $R_{\eta\eta}(t)$ is zero for big lag values, it can be seen that when T' is large, (20) results in

$$\sigma^2_{\hat{m}_0} \approx \frac{2}{T'}\int_{-\infty}^{\infty} R^2_{\eta\eta}(t)dt \tag{21}$$

which, by virtue of the Wiener–Khintchine theorem (7) and Parseval's theorem, can be restated as

$$\sigma^2_{\hat{m}_0} \approx \frac{1}{2T'}\int_{-\infty}^{\infty} S^2_{\eta\eta}(f)df \tag{22}$$

or, using symmetry of the spectrum

$$\sigma^2_{\hat{m}_0} \approx \frac{1}{T'}\int_{0}^{\infty} S^2_{\eta\eta}(f)df. \tag{23}$$

Equation (23) is the formulation referred to in [1]. Logically, when m_0 is estimated over a very long period T' of the signal, each estimate is always almost exactly equal to m_0, and hence, the estimator variance tends to zero (in $1/T'$). In contrast, when considered over a shorter time period, individual m_0 estimates can differ significantly from their long-term average m_0.

The fact that short-term m_0 estimates exhibit a strong variability, compared to longer term estimates, can be illustrated by means of real sea data. Wave elevation data, recorded in the site of Belmullet, in Ireland, at a rate of 1.28 Hz, have been provided by the Irish Marine Institute for the year 2010. For the sake of illustration, a specific time period of 24 h is chosen, during which the wave conditions show very little evolution so that the wave elevation process can be more easily pictured as a stationary Gaussian process, in spite of the relatively long duration considered. The 24 h starting on March 28, 2010, at 2 A.M., meet such requirements, as illustrated in Fig. 8, where it can be seen that the three-hourly wave spectrum undergoes very little change throughout the day.

Fig. 9 shows how the variance estimate $\hat{m}_0$ varies more when considered over a short duration, compared to a longer duration. When estimated every three hours, each $\hat{m}_0$ remains close to the 24-h average (in accordance with the weak variability of the three-hourly spectrum, pictured in Fig. 8). In contrast, $\hat{m}_0$ measured in every 10 min shows significant variability compared to the 24-h average.

Of course, in practice, the wave conditions (characterized by the wave spectrum) are never perfectly stationary, since the meteorological conditions do not stop evolving. As mentioned in Section II, it is important to keep in mind that, for the wave elevation process to be considered as stationary, the duration under study must be small, compared to the rate at which meteorological conditions evolve.

Fig. 10 shows, in each 3-h window, the empirical variance of the 10-min m_0 estimate (i.e., all the 18 10-min $\hat{m}_0$, within each 3-h window, are used to estimate the empirical $\sigma^2_{\hat{m}_0}$). The empirical $\sigma^2_{\hat{m}_0}$ is compared to a theoretical one, obtained by

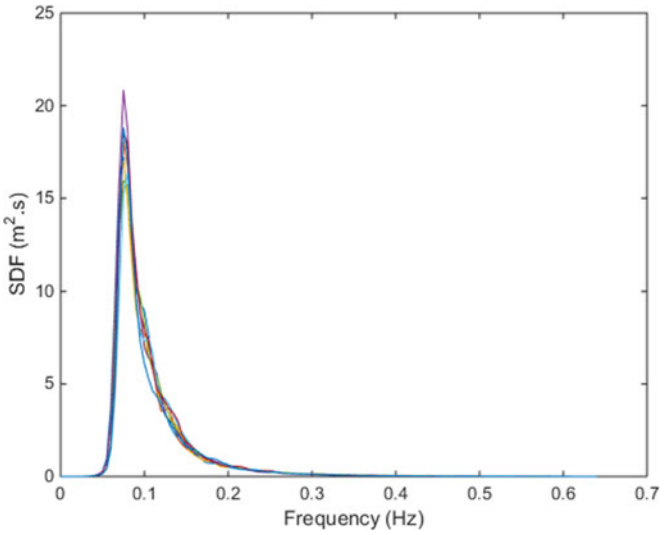

Fig. 8. Eight consecutive three-hourly wave spectra (Belmullet, Ireland, starting March 28, 2010, 02:00).

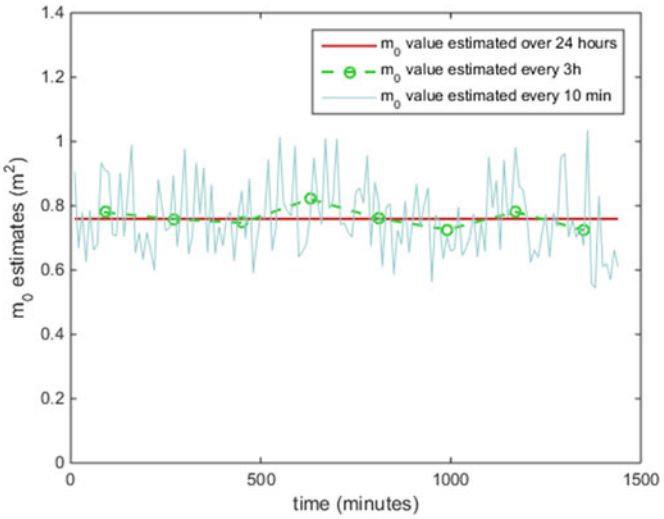

Fig. 9. $\hat{m}_0$ estimated over 24 h, every 3 h and every 10 min (Belmullet, Ireland, starting March 28, 2010, 02:00).

applying (23) to each three-hourly spectrum for $T' = 10$ min. Assuming that the sea state is stationary over the whole day, the empirical and theoretical $\sigma^2_{\hat{m}_0}$ are also computed for the whole 24 h of data (again for $T' = 10$ min). It can be seen that the empirical $\sigma^2_{\hat{m}_0}$, estimated every 3 h, does not exactly match the theoretical one, which can be attributed to two reasons. First, the empirical $\sigma^2_{\hat{m}_0}$ is estimated based on a limited number of points (18 in each 3 h of data) so that it exhibits some variability compared to its average value (which is better approximated by the 24-h value). Second, the sea condition is never exactly stationary so that $\sigma^2_{\hat{m}_0}$ presents some variability, not only due to short-term estimations, but also due to the variability of the sea state (relatively small in this dataset). This second effect is reflected in the 24-h empirical $\sigma^2_{\hat{m}_0}$ being slightly higher than the theoretical one, which would be obtained if the sea conditions were perfectly stationary.

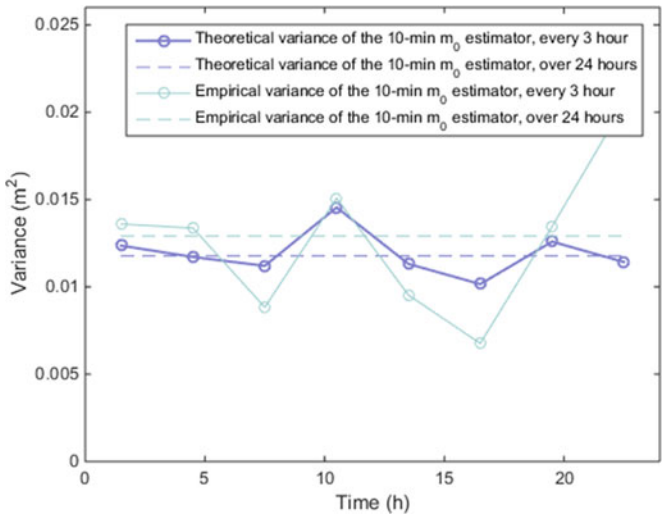

Fig. 10. Theoretical and empirical variance of the m_0 estimate computed every 10 min (Belmullet, starting March 18, 2010, 08:00).

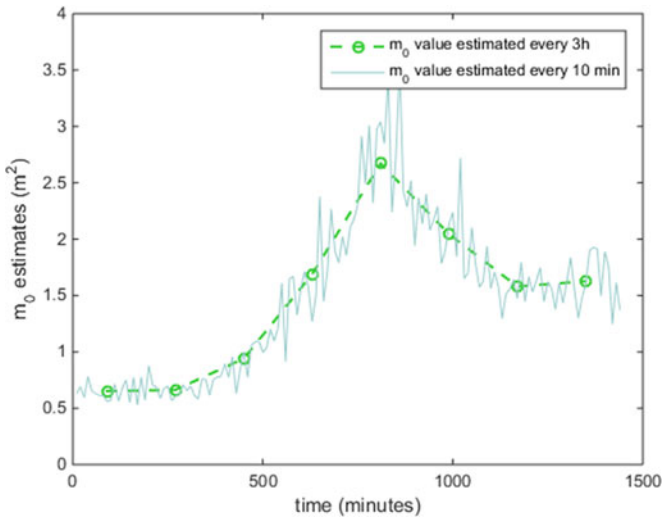

Fig. 11. $\hat{m}_0$ estimated every 3 h and every 10 min (Belmullet, starting March 18, 2010, 08:00).

To illustrate the difference between the variability due to the change in wave conditions (i.e., in the wave spectrum) and the variability of the m_0 estimate due to finite-duration sampling, Fig. 11 shows another example, also recorded at the Belmullet site, in which the meteorological conditions are strongly evolving. It can be seen that:

1) the three-hourly $\hat{m}_0$ estimate varies relatively slowly, which corresponds to the gradual change of the wave spectrum as a result of the weather evolution;
2) in contrast, $\hat{m}_0$, estimated every 10 min, shows an additional, "noisy" variability, which adds to the slow pattern resulting from the weather evolution. As illustrated earlier in Fig. 9, the noisy variability would exist even if the weather were not significantly evolving, and is the result of recording finite-duration samples.

In coherence with (23), $\mathrm{var}[\hat{m}_0]$ is larger in more energetic sea states. Similarly to Fig. 10, Fig. 12 shows, in each 3-h window, the empirical and theoretical variances of the 10-min m_0 estimate. Empirical results differ from theoretical ones more significantly than in Fig. 10, which can be explained by the sea state evolving rapidly, thus giving the empirical $\hat{m}_0$ additional variability within each 3-h period.

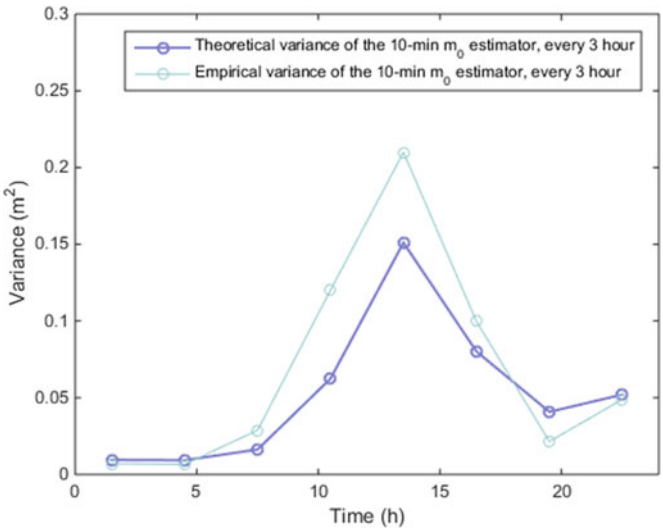

Fig. 12. Theoretical and empirical variance of the m_0 estimate computed every 10 min (Belmullet, Ireland, starting March 18, 2010, 08:00).

As seen in Figs. 10 and 12, the main limitation of empirical observations is that it is impossible to perfectly separate the effects of the sea state evolution from those due to the limited time duration over which spectral estimates are calculated. Overall, it is difficult to quantify accurately how the empirical statistical properties of an actual sea (such as $\mathrm{var}[\hat{m}_0]$) should compare to theoretical ones, and some degree of discrepancy should always be expected between empirical and theoretical results. Nevertheless, real sea observations still clearly validate, at least qualitatively, the key points of this section.

B. m_0 Estimator With Random Amplitude Scheme and Deterministic Amplitude Scheme

Given N' generated points $y_n, n \in \{1, \ldots, N'\}$, the time-domain variance estimator is given by

$$\hat{m}_0 = \frac{1}{N'} \sum_{n=1}^{N'} y_n^2. \tag{24}$$

Alternatively, it could be considered that the generated points can be interpolated, and that an estimate of m_0 in integral form, similar to (19), is derived.

Let us first recall from Section III that, with RAS, the simulated process is Gaussian, with autocorrelation R_{yy}, identical to $R_{\eta\eta}$ until R_{yy} repeats itself. Therefore, taking T' inside the range within which R_{yy} is valid (see Fig. 7), the exact same equation as (18) is derived, and since $R_{yy} = R_{\eta\eta}$, the value of $\sigma^2_{\hat{m}_0}$ with the simulated process is exactly the same as with the true process.

More generally, for both RAS and DAS, it is possible to derive an analytical expression for $\sigma^2_{\hat{m}_0}$ estimated over any T',

but the corresponding calculations would be unnecessary bulky for this paper. Instead, it is simple, and particularly interesting, to consider the specific case where m_0 is estimated over the whole period of the simulated process so that $\Delta f = 1/T = 1/(N\Delta f)$ and $T' = T$. In the following, the probability law followed by $\hat{m}_0$ is derived analytically, both in the RAS and DAS cases.

1) With Random Amplitude Scheme: Let us define $z_k, k \in \{1, \ldots, N\}$ as follows:

$$\begin{cases} z_0 = 0 \\ z_k = \dfrac{N}{2}(a_k - \mathrm{i}b_k), \quad \text{for } k \in \left\{1, \ldots, \dfrac{N}{2} - 1\right\} \\ z_{\frac{N}{2}} = 0 \\ z_k = z^*_{N-k}, \qquad\qquad \text{for } k \in \left\{\dfrac{N}{2} + 1, \ldots, N - 1\right\} \end{cases} \tag{25}$$

where a_k and b_k, $k \in \{1 \ldots N/2\}$, are chosen as independent, normally distributed random variables with zero mean and variance $S_{\eta\eta}(f_k)\Delta f$, and * denotes complex conjugate.

Assuming $S_{\eta\eta}(f_{\max}) = S_{\eta\eta}((N/2)\Delta f) = 0$ (which can be obtained by making Δt smaller for example), it is easily shown that, with RAS, y_n is generated as

$$y_n = \frac{1}{N}\sum_{k=0}^{N-1} z_k \mathrm{e}^{\mathrm{i}2\pi\frac{kn}{N}}. \tag{26}$$

Thus, y is the inverse discrete Fourier transform (DFT) of z. Applying Parseval's theorem (see, for example, [10]), we have that

$$\sum_{n=1}^{N} |y_n|^2 = \frac{1}{N}\sum_{k=0}^{N-1} |z_k|^2 = \frac{N}{2}\sum_{k=1}^{\frac{N}{2}} (a_k^2 + b_k^2) \tag{27}$$

so that

$$\hat{m}_0 = \frac{1}{2}\sum_{k=1}^{\frac{N}{2}} (a_k^2 + b_k^2). \tag{28}$$

As a consequence, the average value of the m_0 estimator is

$$\mu_{\hat{m}_0} = \sum_{k=1}^{\frac{N}{2}} S_{\eta\eta}(f_k)\Delta f \tag{29}$$

which corresponds to the Riemann approximation of (10).

The probability law, followed by the random scalar $\hat{m}_0$, is a quadratic form on a Gaussian random vector $X \in \mathbb{R}^N$

$$\hat{m}_0 = \frac{1}{2}X^T X \tag{30}$$

where

$$\begin{cases} X_k = a_k, \quad \text{for } k \in \left\{1, \ldots, \dfrac{N}{2}\right\} \\ X_k = b_k, \quad \text{for } k \in \left\{\dfrac{N}{2} + 1, \ldots, N\right\}. \end{cases}$$

The variance of such a distribution is $\sigma^2_{\hat{m}_0} = 1/4 \times 2\mathrm{tr}(\Sigma_X^2)$, where Σ_X is the variance-covariance matrix of the Gaussian random vector X (see, for example, [11]) and tr denotes the trace. This yields to

$$\sigma^2_{\hat{m}_0} = \sum_{k=1}^{N/2} S^2_{\eta\eta}(f_k)\Delta f^2. \tag{31}$$

Equation (31) can also be formulated as

$$\sigma^2_{\hat{m}_0} = \frac{1}{T}\sum_{k=1}^{N/2} S^2_{\eta\eta}(f_k)\Delta f \tag{32}$$

which, when Δf is small, is coherent with (23).

Assuming that N is big enough, which is the case for T values above several tens of seconds, the sum in (32) will remain almost constant as N increases [and approximately equal to the integral of (20)]. Thus, when T increases, $\sigma^2_{\hat{m}_0}$ decreases in $1/T$. Then, RAS reproduces the variability of $\hat{m}_0$ due to finite-duration sampling of the underlying Gaussian process.

2) With Deterministic Amplitude Scheme: The results for the DAS case can now be derived in a similar way. Indeed, it suffices to view y as the result of an inverse DFT, as in (25), except that, this time, a_k and b_k are generated as

$$\begin{aligned} a_k &= \cos\phi_k \sqrt{2\Delta f S_{\eta\eta}(f_k)} \\ b_k &= -\sin\phi_k \sqrt{2\Delta f S_{\eta\eta}(f_k)} \end{aligned} \tag{33}$$

where $\forall k \in \{1, \ldots, N/2\}$, and ϕ_k is randomly chosen following a uniform distribution in $[0; 2\pi]$.

As a result, it stems from (28) that $\hat{m}_0$ is not a random variable anymore and takes the same value at each realization as

$$\hat{m}_0 = \sum_{k=1}^{\frac{N}{2}} S_{\eta\eta}(f_k)\Delta f \tag{34}$$

and

$$\sigma^2_{\hat{m}_0} = 0. \tag{35}$$

This is a particular illustration of the fact that, as mentioned in the introduction, DAS preserves all spectral moments at each realization.

C. $\bar{P}_{\mathrm{PTO}}$ Estimator for a Linear Wave Energy Converter

In this section, a linear WEC model subject to simulated incident waves is considered. For the sake of simplicity, it is assumed that the WEC is constrained to heave motion only. Furthermore, the PTO is modeled as a linear damper so that the instantaneous power captured by the PTO is given by $P_{\mathrm{PTO}}(t) = C_{\mathrm{PTO}}\dot{z}^2(t)$, where $\dot{z}(t)$ denotes the WEC heave velocity.

Thus, with N measured or simulated points for the heave velocity, the estimator for the average WEC power output is given by

$$\hat{P}_{\mathrm{PTO}} = C_{\mathrm{PTO}}\sum_{n=1}^{N} \dot{z}_n^2. \tag{36}$$

Similarly to [1], let us define $\overline{H_{\dot{z}\eta}(f)}$ the linear, frequency-domain complex transfer function that relates the (input)

free-surface elevation to the (output) WEC heave velocity. As mentioned in [1], the output of a linear system driven by a Gaussian process is a Gaussian process. Furthermore, the SDF of the resulting Gaussian process—in our case $S_{\dot{z}\dot{z}}(f)$—is given by

$$S_{\dot{z}\dot{z}}(f) = S_{\eta\eta}(f)|\underline{H_{\dot{z}\eta}}|^2(f). \tag{37}$$

Considering the WEC in the true Gaussian ocean waves, $\dot{z}$ is then a Gaussian process, from where it follows, similarly to Section IV-A, that finite-length estimates $\hat{P}_{\mathrm{PTO}}$ present some variability with respect to the long-term average $\bar{P}_{\mathrm{PTO}}$. The same results as in Section IV-A can be derived, in particular (23), replacing $S_{\eta\eta}$ with $S_{\dot{z}\dot{z}}$.

We are now interested in the properties of the *simulated* WEC dynamics, either with RAS or with DAS. Since the system is linear, its steady-state response to a sum of orthogonal frequency components is the sum of the responses to each of the frequency components. The steady-state response, e.g., in heave velocity, to a specific frequency component $A_k\cos(2\pi f_k t + \phi_k)$, is a sinusoid with the same frequency f_k, amplitude $A_k|\underline{H_{\dot{z}\eta}}|(f_k)$, and a phase shift $\Delta_\phi(f_k)$ added to ϕ_k.

Let us now simulate the device steady-state response, either with DAS or with RAS. As shown in (1) and (3), in both cases, the simulated waves can be written as follows, the only difference being the way A_k are generated:

$$y_n = \sum_{k=1}^{M/2} A_k\cos(2\pi f_k t_n + \phi_k). \tag{38}$$

The total steady-state heave velocity response of the device is then given by

$$\begin{aligned}\dot{z}_n &= \sum_{k=1}^{N/2} A_k|\underline{H_{\dot{z}\eta}}|(f_k)\cos(2\pi f_k t_n + \phi'_k)\\ &= \sum_{k=1}^{N/2} A'_k\cos(2\pi f_k t_n + \phi'_k)\end{aligned} \tag{39}$$

where $\phi'_k = \phi_k + \Delta_\phi(f_k)$ (phases ϕ'_k then also follow a uniform distribution in $[0; 2\pi]$); and $A'_k = A_k|\underline{H_{\dot{z}\eta}}|(f_k)$. If η is generated through RAS, then A'_k are Rayleigh distributed with variance $|\underline{H_{\dot{z}\eta}}|^2(f_k)S_{\eta\eta}(f_k)\Delta f = S_{\dot{z}\dot{z}}(f_k)\Delta f$. If η is generated through DAS, then A'_k are equal to $|\underline{H_{\dot{z}\eta}}|(f_k)\sqrt{2S_{\eta\eta}(f_k)\Delta f} = \sqrt{2S_{\dot{z}\dot{z}}(f_k)\Delta f}$.

In any case, in (39), one can recognize a harmonic superposition method (either RAS or DAS) applied to the heave velocity Gaussian process characterized by its SDF $S_{\dot{z}\dot{z}}(f)$: either RAS, if the A'_k are Rayleigh distributed, or DAS, if the A'_k are deterministic. In other words, using RAS (respectively DAS) to generate y and then simulate the device steady-state heave velocity response is equivalent to a direct application of RAS (respectively DAS) to generate heave velocity time series from the heave velocity SDF, $S_{\dot{z}\dot{z}}(f)$.

Using the results of Section IV-B, it is now easy to derive the properties of the $\bar{P}_{\mathrm{PTO}}$ estimator.

1) With Random Amplitude Scheme:

$$\hat{P}_{\mathrm{PTO}} = \frac{C_{\mathrm{PTO}}}{2}\sum_{k=1}^{\frac{N}{2}}(a'^{2}_{k} + b'^{2}_{k}) \tag{40}$$

where a'_k and b'_k are independent zero mean, normally distributed with variance $S_{\dot{z}\dot{z}}(f_k)\Delta f$.

The average value of the $\bar{P}_{\mathrm{PTO}}$ estimator is

$$\mu_{\hat{P}_{\mathrm{PTO}}} = C_{\mathrm{PTO}}\sum_{k=1}^{\frac{N}{2}} S_{\dot{z}\dot{z}}(f_k)\Delta f \tag{41}$$

and the variance of the estimator is

$$\sigma^2_{\hat{P}_{\mathrm{PTO}}} = \frac{C_{\mathrm{PTO}}}{T}\sum_{k=1}^{N/2} S^2_{\dot{z}\dot{z}}(f_k)\Delta f. \tag{42}$$

2) With Deterministic Amplitude Scheme:

$$\hat{P}_{\mathrm{PTO}} = C_{\mathrm{PTO}}\sum_{k=1}^{\frac{N}{2}} S_{\dot{z}\dot{z}}(f_k)\Delta f \tag{43}$$

and

$$\sigma^2_{\hat{P}_{\mathrm{PTO}}} = 0. \tag{44}$$

With DAS, the average power estimator $\hat{P}_{\mathrm{PTO}}$ takes the same value in every simulation.

V. Nonharmonic Superposition Methods

It may be considered that for long simulations, the computational cost of either DAS or RAS is prohibitive. However, decreasing the number of frequency components below $N/2$ by increasing the frequency step is not a suitable solution, since it makes the generated signal (and its autocorrelation) repeat itself within the simulation window.

Therefore, other methods, also based on the superposition of sinusoids, have been suggested to avoid signal repetition. Their basic principle is to choose the frequencies in a nonharmonic way [12] so that even with a number of frequency components much smaller than $N/2$, the signal does not repeat itself within the simulation window. Such methods could be used either with random or deterministic amplitudes of the nonharmonic wave components and, therefore, can be referred to as NHRAS or NHDAS.

Based on the following two simple arguments, using NHRAS or NHDAS is not recommended.

1) Similarly to DAS, the vector generated through NHDAS is not Gaussian and, thus, cannot properly model the target Gaussian vector.
2) Similarly to RAS, the vector generated through NHRAS is Gaussian. However, this time, the Gaussian vector is degenerate, since it is of size N and it is obtained as a linear combination of $M \ll N$ independent, standard Gaussian random variables. Therefore, the variance-covariance matrix of the generated vector cannot be identical to the variance-covariance matrix $\Sigma_{\eta\eta}$ of the true sampled signal (11).

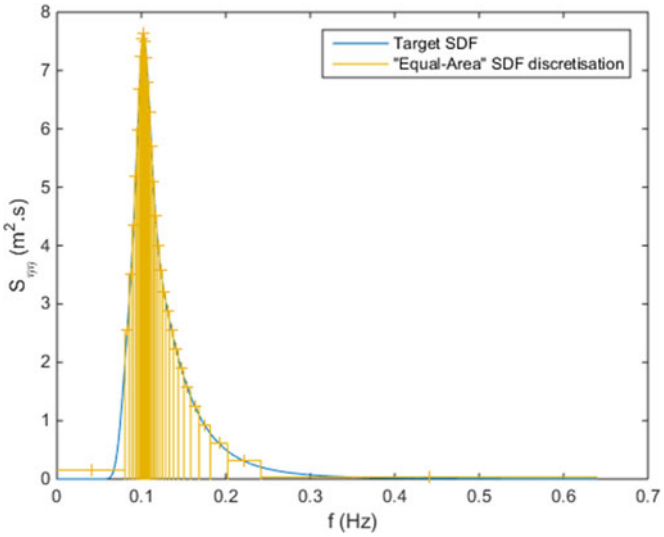

Fig. 13. Discretization of the target SDF following the EA methodology.

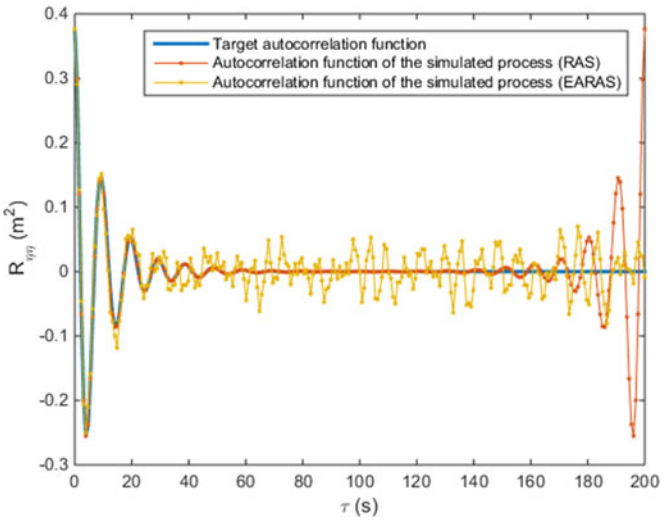

Fig. 14. Autocorrelation functions of the target Gaussian process, RAS-simulated process, and EARAS-simulated process.

For illustration, the following paragraphs will consider in more detail the random-amplitude version of the so-called equal-area (EA) method, which consists of choosing frequency steps so that the spectral energy at each frequency component is the same (see, for example, [12] or [13, ch. 10]). The total spectral energy m_0 is divided into $M/2$ equal parts so that

$$\Delta E = \frac{2m_0}{M}. \tag{45}$$

Accordingly, the frequency range $[0; 1/(2\Delta t)]$ is divided into $M/2$ intervals, defined as $I_k = [f_k - ((\Delta f_k)/2); f_k + ((\Delta f_k)/2)], k \in \{1, \ldots, M/2\}$, and such that (see Fig. 13)

$$\forall k \in \left\{1, \ldots, \frac{M}{2}\right\}, \int_{I_k} S_{\eta\eta}(f)df = \Delta E. \tag{46}$$

Then, EARAS is formulated as

$$\eta_{t_i} = \sum_{k=1}^{M/2} a_k \cos(2\pi f_k t_i) + b_k \sin(2\pi f_k t_i) \tag{47}$$

where a_k and b_k are chosen as independent, normally distributed random variables with zero mean and variance ΔE.

A. Autocorrelation Function

Using similar demonstrations to those presented in Sections III and IV, it can be shown that the variance-covariance matrix of the Gaussian vector obtained through EARAS has the same structure as in (14); however, this time, the sequence s_j is different from the target autocorrelation function (otherwise, the Gaussian vector would not be degenerate). More precisely, the discrete autocorrelation sequence is given by

$$\forall j \in 0, \ldots, N-1, s_j = \Delta E \sum_{k=1}^{\frac{M}{2}} \cos(2\pi f_k j \Delta t). \tag{48}$$

Equation (48) can also be formulated as

$$s_j = \frac{1}{2} \sum_{\substack{k=-\frac{M}{2} \\ k\neq 0}}^{\frac{M}{2}} S_k \mathrm{e}^{\mathrm{i}2\pi f_k j \Delta t} \Delta f_k \tag{49}$$

where $S_k = \Delta E/\Delta f_k$. For small j's, (49) can be seen as a Riemann approximation of integral (8); however, all the components of the sum are periodic, with different periods, but with the same magnitude ΔE. For lag values well inside the simulation duration, the discrete ACVF is significantly polluted, as shown in Fig. 14 (and experimentally pointed out in [14]). In the EA example shown on Figs. 13 and 14, the frequency range is divided into $M/2 = 30$ intervals. By increasing the number of intervals, the amplitude of the noisy oscillations in the autocorrelation function decreases, but then, the only benefit of using EARAS, which was to use fewer frequency components than RAS, is lost.

It is interesting to note that, for lag values close to M, the ACVS obtained from the EARAS method more closely matches the correct one than RAS does. However, with RAS, it is still possible to isolate the part of the signal (e.g., the first) where the ACVF is not polluted while, with EARAS, the ACVF remains polluted, regardless of the part of the signal considered.

B. m_0 Estimator

If EARAS allowed for simulating arbitrarily long signals from only a limited number of frequency components, one would expect that $\hat{m}_0$, estimated from the generated signals, would exhibit the same properties as $\hat{m}_0$ estimated from the true process. In particular, for big values of T', $\sigma^2_{\hat{m}_0}$ should follow (23).

Let us consider a signal generated through EARAS. Let us also assume that the signal is interpolated, so that m_0 can be estimated in integral form as in (19). One can show that the variance of the m_0 estimator is given in a similar way to (20), with $R_{\eta\eta}$ replaced with the (polluted) autocorrelation function

of the generated signal as follows:

$$\sigma^2_{\hat{m_0}} = \frac{2}{T'}\int_{-T'}^{T'}\left(1-\frac{|t|}{T'}\right)R^2_{yy}(t)dt. \tag{50}$$

$R_{yy}(\tau)$ is a continuous-time version of (48) and (49)

$$R_{yy}(\tau) = \frac{\Delta E}{2}\sum_{\substack{k=-\frac{M}{2}\\ k\neq 0}}^{\frac{M}{2}}\cos(2\pi f_k \tau). \tag{51}$$

Injecting (51) into (50), and carrying out the integration analytically, yields to

$$\sigma^2_{\hat{m_0}} = \frac{\Delta E^2}{T'^2}\sum_{\substack{k=-\frac{M}{2}\\ k\neq 0}}^{\frac{M}{2}}\sum_{\substack{l=-\frac{M}{2}\\ l\neq 0}}^{\frac{M}{2}}\Lambda_{k,l}(T') \tag{52}$$

where

$$\forall(k,l),\Lambda_{k,l} = \begin{cases}\frac{1-\cos\left(2\pi(f_k+f_l)T'\right)}{\left(2\pi(f_k+f_l)\right)^2}, & \text{if } k\neq -l\\ \frac{T'^2}{2}, & \text{if } k=-l.\end{cases} \tag{53}$$

For a fixed frequency discretization $\{f_1,\ldots,f_{M/2}\}$, it is clear from (53) that all the terms inside the double sum in (52) are bounded, except those such that $k=-l$. Therefore, when T' becomes large, in (52) all the terms such that $k\neq l$ tend to zero, leaving only

$$\sigma^2_{\hat{m_0}} \approx \frac{M}{2}\Delta E^2. \tag{54}$$

Reminding that $(M/2)\Delta E = m_0$, (52) can be rewritten as

$$\sigma^2_{\hat{m_0}} \approx \frac{2}{M}m_0^2. \tag{55}$$

Then, instead of fading out to zero following a law in $1/T'$, when T' becomes large $\text{var}[\hat{m}_0]$ converges to a constant value depending only on m_0 and on the number of frequency components $M/2$.

C. Conclusion

In view of the arguments presented in the rest of Section V, the following can be said.

1) NHDAS and NHRAS do not compare favorably to DAS and RAS respectively in terms of intrasimulation properties, since the statistical relationships between simulation points are incorrectly modeled;
2) unlike RAS, the intersimulation properties of NHRAS do not accurately reflect finite-duration records of a Gaussian sea, presented in Section IV-A.

The computational gain of using NHRAS or NHDAS is then clearly obtained at the expense of the statistical properties of the generated signal. It does not seem possible to simulate the correct signal statistical properties without including at least $N/2$ frequency components (for a constant cutoff frequency $1/2\Delta t$).

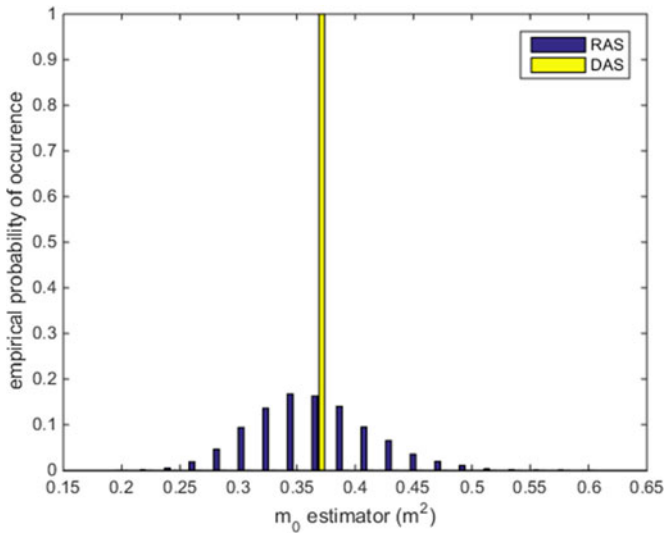

Fig. 15. Empirical distribution of $\hat{m}_0 = (1/N)\sum_{i=1}^{N}\eta_i^2$ obtained from 10 000 simulations of $T = 600$ s.

VI. Numerical Experimental Validation

A. Wave Time-Domain Statistics

In this section, the effect of the simulation method on various wave statistics is illustrated, using a JONSWAP SDF with $H_{m_0} = 2.46$ m ($m_0 = 0.3765$ m^2), $T_p = 9.8$ s and $\gamma = 1.7$. Around 10 000 simulations of $T = 600$ s were run, using both RAS and DAS. In each simulation, individual waves are counted through zero up-crossing, and wave statistics are computed.

Fig. 15 illustrates the theoretical results shown in Section IV-B: While the variance estimator of the finite-length generated signal presents some variability with RAS (and so would be the case if one were measuring real free-surface elevation in a finite duration), it is not the case with DAS, for which the variance estimator of the generated signal always takes the same value exactly equal to m_0. Furthermore, using (31), the theoretical variance of the m_0 estimator with RAS is found to be $\sigma^2_{\hat{m}_0} = 0.0025$ m^2 so that the standard deviation, expressed as a percentage of m_0, is 13.35%, which is confirmed with good accuracy by experimental results (see Table I).

Figs. 16–18 show histograms for wave height statistics in the 10 000 simulations. In each simulation, the average height of the $1/3$ and $1/10$ highest waves is computed, as well as the maximum wave height. For $H_{33\%}$ and $H_{10\%}$, the resulting distributions present a Gaussian-looking shape, with significantly larger spreading for simulations realized through RAS. For both DAS and RAS, the distribution of maximum wave heights exhibits a similar shape and variance.

Fig. 19 shows the histogram of the average wave steepness values, which also presents a Gaussian shape with significantly larger spreading for the RAS simulations.

Finally, Table I summarizes the main results obtained. The results suggest that using DAS does not affect average values for the statistics studied, including extreme values (maximum wave height and steepness of the highest wave). However, the

TABLE I
EMPIRICAL MEAN μ AND PERCENTAGE STANDARD DEVIATION $(100\% \times \sigma/\mu)$ OBTAINED FROM 10 000 SIMULATIONS OF $T = 600$ S

	Mean		Standard deviation (%)	
	RAS	DAS	RAS	DAS
Variance estimator $(\sigma^2_{\hat{m}_0}, m^2)$	0.3769	0.3765	13.2	0.0
Average height of the 1/3 highest waves $(H_{33\%}, \text{m})$	2.333	2.337	7.1	1.9
Average height of the 1/10 highest waves $(H_{10\%}, \text{m})$	2.888	2.898	8.0	4.1
Maximum wave height $(H_{\max}, \text{m})$	3.562	3.590	12.4	10.8
Average wave period $(T_{\text{mean}}, \text{s})$	7.350	7.354	4.6	3.6
Average wave steepness (S_{mean})	0.0192	0.0192	5.7	3.9
Average steepness of the 1/3 highest waves $(S_{H\,33\%})$	0.0210	0.0210	7.7	4.7
Average steepness of the 1/10 highest waves $(S_{H\,10\%})$	0.0295	0.0295	17.8	16.6
Steepness of the highest wave $(S_{H\,\max})$	0.0311	0.0312	22.7	21.7

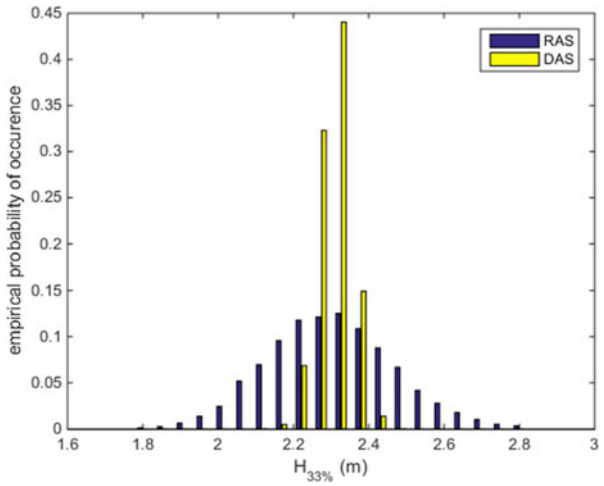

Fig. 16. Empirical distribution of $H_{33\%}$ obtained from 10 000 simulations of $T = 600$ s.

results obtained for $H_{33\%}$, $H_{10\%}$, T_{mean}, and S_{mean} show that DAS leads to a significant underestimation of the variance of the corresponding wave statistics.

In practice, as illustrated in Section IV-A, an actual, finite-duration wave record in a given sea-state could present wave statistics that depart significantly from their mean, long-term values that would be obtained by using an infinitely long wave record of the same sea state. While RAS reproduces this effect with the appropriate magnitude, DAS fails in doing so.

B. Power Production Statistics

This section is dedicated to the effect of the simulation method upon power production statistics for a linearly modeled WEC. The methodology, and results presented, is very similar to the

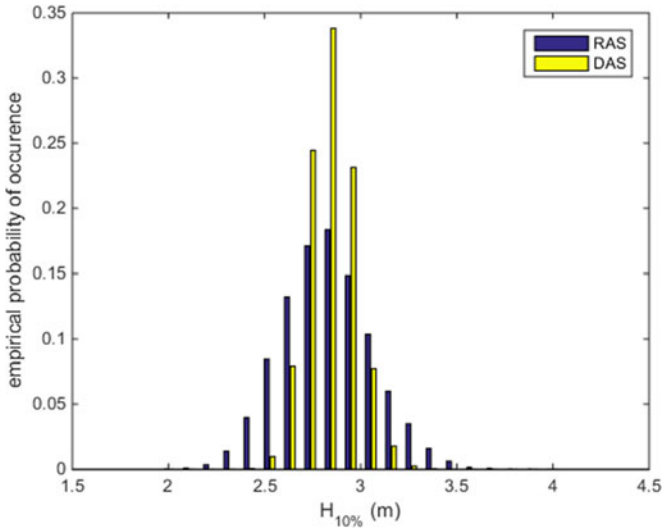

Fig. 17. Empirical distribution of $H_{10\%}$ obtained from 10 000 simulations of $T = 600$ s.

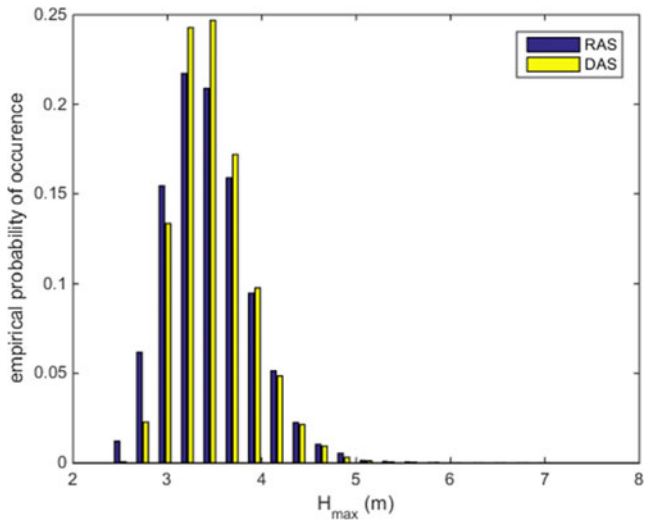

Fig. 18. Empirical distribution of $H_{\max}$ obtained from 10 000 simulations of $T = 600$ s.

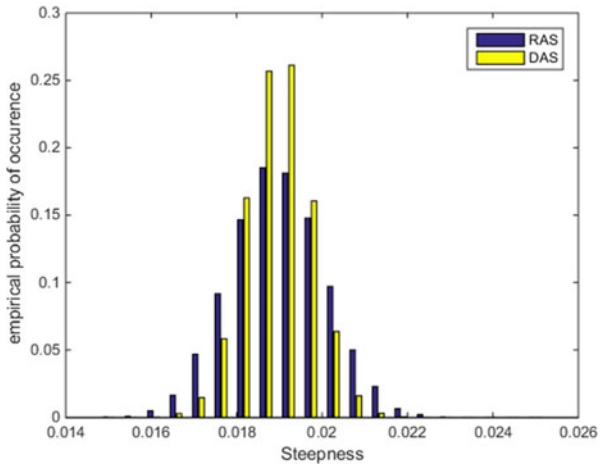

Fig. 19. Empirical distribution of S_{mean} (average wave steepness) obtained from 10 000 simulations of $T = 600$ s.

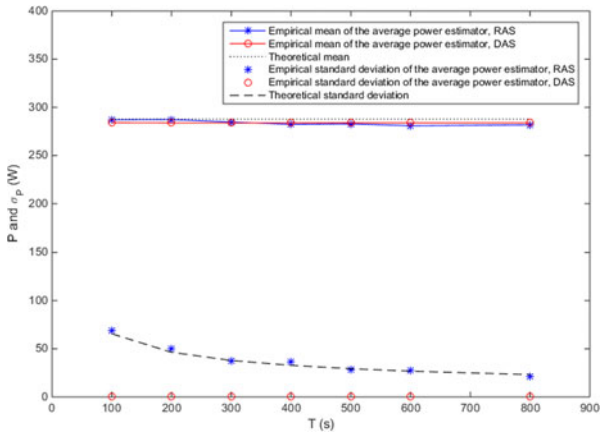

Fig. 20. $\bar{P}_{\mathrm{PTO}}$ estimator and its variance with RAS and DAS for different simulation durations.

ones shown in [1]; therefore, this section will be kept short. However, unlike in [1], here it is confirmed, through numerical experiments, that the power estimator presents zero variance when DAS is used to generate the incident wave, as was demonstrated in Section IV-C.

The WEC considered is a cylinder constrained to heave motion. As in the linear model of [1], the time-domain equation of motion takes the form of the Cummins integro-differential equation and the PTO is modeled as a linear damper.

Using both RAS and DAS, the device is simulated in the sea state studied in Section VI-A, for different time durations. About 100 simulations are run for each time duration and wave simulation method. The empirical mean and variance of the average power estimator ($\hat{P}_{\mathrm{PTO}}$) are computed and compared with theoretical values. The results are shown in Fig. 20.

An important point to mention here is the way the transient part of the simulation is dealt with. Indeed, for (35) to be true, $\hat{P}_{\mathrm{PTO}}$ has to be computed over the steady-state signal only. To achieve this, a transient time is introduced at the beginning of the simulations so that $T_{\mathrm{tot}} = T_{\mathrm{transient}} + T$. However, the number of frequencies is chosen so that the signal is periodic, with period T, i.e., $\Delta f = 1/T$. The part of the η signal corresponding to the transient time then repeats itself at the end of the total signal, as illustrated in Fig. 21. But the transient part is discarded when computing $\hat{P}_{\mathrm{PTO}}$. This way, the average power output estimator is evaluated over a whole period T of the generated signal. The results of Fig. 20 agree well with theoretical predictions of Section IV. With RAS, the variance of the average power output estimator follows the $1/T$ law predicted by theory (and its standard deviation follows the corresponding $1/\sqrt{T}$ law). With DAS, the value of the average power output estimator is the same, regardless of the choice of phases, which results in a zero variance of the estimator, in accordance with theory. Therefore, RAS enables the accurate representation of the fluctuations of short-term device performance around the average, while DAS directly gives the average value in only one simulation.

Let us note that for the DAS to result in zero variance of the power estimator—and then an immediate accurate estimate of the average power estimator—it is essential that the wave signal generated is of period T and not T_{tot} (as is the case in [1]): In the latter case, the distribution of the total signal energy between the two parts of the signal ($T_{\mathrm{transient}}$ and T) depends on the choice of phases so that the $\bar{P}_{\mathrm{PTO}}$ estimator does not present negligible spreading any more.

Finally, it can be seen from Fig. 20 that the time-domain numerical estimates of $\bar{P}_{\mathrm{PTO}}$ with DAS do not exactly coincide with their theoretical value. The slight offset can be attributed to the numerical approximations inherent to numerical integration. In particular, in Cummins equation, the radiation force convolution product may be particularly sensitive to the integration step and to the length of the convolution domain.

VII. Discussion

Whatever the simulation method chosen, it is preferable to have some insight on the consequences that this decision will have on the statistical properties of the simulation results. Therefore, we believe that this study can be useful to help researchers and engineers make informed decisions with regard, for example, to the number and length of the simulations necessary to obtain an accurate power estimate, or to comprehensively cover the device operational space.

Based only on the arguments presented in Section III, it is not obvious that DAS should be simply discarded as a simulation method. RAS is certainly a more faithful representation of a Gaussian sea than DAS, since it reproduces the fact that the statistics of a finite-duration wave record deviate from the long-term statistics that would be obtained with an infinite-length record.

But it could also be said that DAS is more representative of a given wave spectrum, since statistics obtained from only one simulation are closer to the long-term statistic that would be obtained from an infinite-length record—it is the case above all for spectral moments that are exactly preserved at each realization. Intuitively, it means that with DAS, "big" waves present in the simulation are somehow balanced by "small waves" so that the wave height distribution over a finite-duration simulation is always close to the long-term wave height distribution. In contrast, with RAS, it is possible that in some simulations, "big" waves, (respectively "small" waves) are significantly over- or underrepresented compared to the long-term wave height distribution. DAS could then be considered as a quicker way than RAS to capture the characteristics of a given sea spectrum.

Ultimately, the choice of simulation method should be governed by the intended objectives.

A. WEC Performance Estimation

At least in the case of a linear WEC, DAS immediately gives an accurate, unbiased estimate of the power output, provided that the latter is evaluated over the whole period of the generated signal. Furthermore, results presented in [1] suggest that, even in the case of a weakly nonlinear WEC, $\hat{P}_{\mathrm{PTO}}$ values from DAS remain unbiased and have a modest spread compared to the RAS case. Hence, in the situation of a linear or weakly nonlinear WEC model, DAS is the quickest method to obtain a reliable estimate of the WEC average power output. However, it should

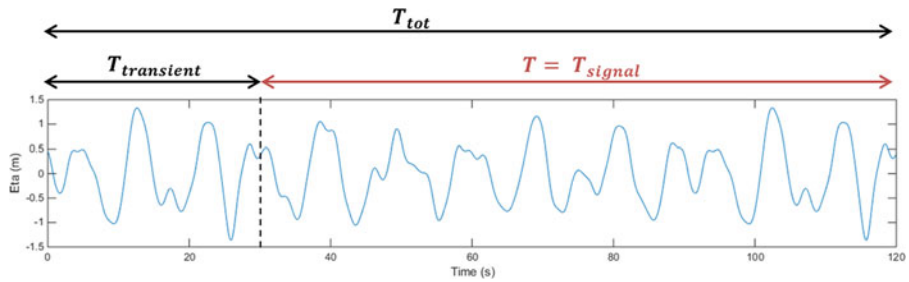

Fig. 21. Methodology to remove the transient part of the simulation.

be ascertained whether DAS resulting in unbiased estimates remains true for configurations presenting strong nonlinearities: perhaps situations could be imagined where, due to nonlinear dynamics, control strategy, and position or velocity constraints, DAS produces biased estimates of the average power output.

In any case, DAS does not give any idea of the spread of the WEC performance considered over a finite duration in an actual sea. In contrast, the statistical information provided by running several simulations with RAS can be relevant, for example, at the design stage, when comparing two WEC designs and/or control strategies; running only one simulation of each of the two configurations compared may not be sufficient to assess which one performs the best. It may also appear that the performance of one WEC configuration, in a given sea state, presents much more variability than the other configuration. WEC performance variability should enter into account when choosing the appropriate WEC design. Only simulations through RAS that represent the true variability of the short-term statistics can properly highlight such effects.

Within the scope of power assessment studies, even if DAS always gave unbiased average power estimates, it would not properly represent the wave power output variability, which could have some impact for grid integration studies for example. Let us consider a power assessment study in which the WEC is simulated in half-hourly wave spectra. The sea condition evolves relatively slowly over time. If DAS is used to simulate the WEC in each sea state, and if the WEC model is linear, the half-hourly average power value obtained evolves as slowly as the wave condition (thick line in Fig. 22). The history of half-hourly power obtained this way would then represent a sort of "average case" for each successive spectrum. But in real conditions, half-hourly records would present more variability, and so would half-hourly average power values. Only simulations through RAS can account for the realistic half-hourly variability (thin lines in Fig. 22). Using the proper simulation method (RAS) is then essential to correctly represent the medium-term variability of absorbed power. Finally, let us note that the "thick curve" in Fig. 22 could be obtained by averaging many of the "thin curves" obtained from half-hourly RAS simulations.

In the operational stage, when WECs will have been deployed at sea, understanding the statistical behavior of the WEC output in a given sea condition, and for a finite duration, will be crucial for online reporting and monitoring, and for power production forecasts. For example, if the wave condition is forecast or measured, say, on a half-hourly basis, also must be the WEC

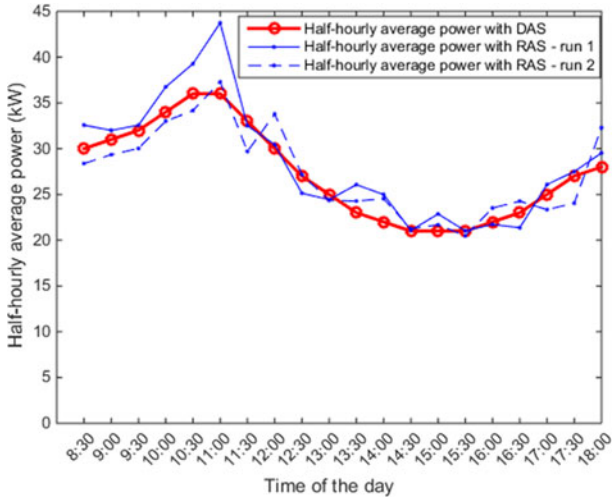

Fig. 22. Illustrative example of half-hourly average power chronicle, with DAS and RAS.

outputs, to forecast power production, or to detect any abnormal performance deviation indicative of incipient damage. In this respect as well, only RAS can properly model and predict the variability of the WEC half-hourly outputs around expected values.

B. Survival Mode

In severe sea conditions, many WECs will be able to stop producing power and to adopt a configuration that preserves them from being significantly damaged. The choice of entering survival mode is based on the expected sea condition, for example, on the value of the significant wave height H_{m_0}. Setting the adequate threshold for survival mode is the result of a trade-off between the objectives of power production maximization and survivability [15]. Eventually, the decision of entering safe mode would depend on the evaluation of the danger presented by a given sea condition to the structural integrity of the device.

Results presented in Section VI-A (Figs. 15–17 in particular) suggest that DAS partly "hides" the possibility of encountering a high density of large waves within a short amount of time (upper tail of the $H_{33\%}$ distribution of Fig. 16 obtained with RAS). Thus, to faithfully represent the possible danger of operating in a given sea condition for a given duration, it could be preferable to run several simulations based on RAS rather than DAS.

TABLE II
SUGGESTED SIMULATION METHOD DEPENDING ON THE OBJECTIVE CONSIDERED AND THE TYPE OF WEC

	WEC model characteristics	
Objective considered	Linear or weakly nonlinear	Strongly nonlinear
Estimate average power output for a given spectrum	DAS	RAS
Model the variability of the WEC performance considered over a finite duration	RAS	RAS
Study complex long-term statistics (e.g., on individual oscillations)	DAS	RAS
Study complex statistics (e.g., on individual oscillations) considered over a finite duration	RAS	RAS

However, it should also be noted that due to a smaller dispersion of results, similarly to power output estimators, DAS is quicker than RAS in giving accurate values for some wave statistics, such as $H_{33\%}$.

The average $H_{\max}$ value (measured over the typical duration of a storm, for example) could allow for assessing the severity of a sea condition, similarly to the so-called most probable maximum individual wave height [16], and hence be used as a criterion to enter survival mode.

$H_{\max}$ can also be used at the WEC design stage to estimate extreme loads on the device. Indeed, extreme loads are likely to correspond to the highest wave H_{ext} encountered throughout the WEC design lifetime. H_{ext} can be estimated, for example, by first determining the most extreme sea state that can likely be encountered at the WEC location, and then, using the maximum wave height $H_{\max}$ that will be observed in this extreme sea state, over a typical storm duration [17]. From this perspective, it can be noted that the $H_{\max}$ histograms, obtained through RAS and DAS, do not show any significant difference (see Fig. 18). However, the question of the most appropriate methodology to assess WEC survivability is outside the scope of this paper.

Finally, let us also stress that statistics on the WEC response similar to the wave height statistics presented in Section VI-A, such as the average value of the 33% or 10% widest WEC oscillation, could also be studied, and would exhibit results analogous to those obtained for wave height statistics, at least with a linear WEC.

C. Computational Time

With modern computers, there is little chance that computational effort could be a significant impediment to the use of RAS or DAS. First of all, the FFT formulations of RAS and DAS allow for a complexity of the order of $N \ln N$, which is only problematic for very large values of N, i.e., with very long simulations and a very refined time step. Furthermore, the computational time required to generate free-surface elevation time series is likely to be negligible, compared to the significant computational cost of many time-domain nonlinear WEC models.

Additionally, there is no obvious reason for running very long simulations of a WEC for the same wave spectrum. In particular, from the point of view of the WEC output statistics, and putting aside the transient time, running a very long RAS-based simulation of length KN ($T_{\text{CPU}} \propto KN \ln KN$) is equivalent to running K shorter RAS-based simulations of length N ($T_{\text{CPU}} \propto KN \ln N$). Therefore, if a very large amount of statistical data (say, N) has to be obtained from a WEC model in a given wave spectrum, it can be beneficial to obtain the desired data through many, relatively short simulations, so that the computational burden due to the wave generation increases proportionally to N, instead of $N \ln N$.

Finally, it is often the case that the desired time step, for the free-surface time series (typically 10^{-3}s), is orders of magnitude smaller than the time step corresponding to the maximum frequency of interest present in the wave spectrum (typically 1 s): $\Delta t \ll 1/(2f_{\max})$. To be able to use FFT to compute the wave elevation, it is necessary to fill-in the SDF with zeros for frequencies between $f_{\max}$ and $1/(2\Delta t)$. But, by doing so, the signal probability space is not extended since, either with RAS or DAS, the additional sinusoidal components have zero amplitude. So, it can be computationally beneficial, and neutral for the signal statistical properties, to first generate a time series through FFT with time step $1/(2f_{\max})$, and then obtain the missing points through a relevant interpolation method. A quick numerical investigation tends to show that, by combining FFT and cubic spline interpolation, the difference with the signal obtained through direct FFT is negligible, and that the computational time can be reduced of at least one order of magnitude. More work would be necessary to accurately quantify the resulting error and computational gain.

VIII. CONCLUSION AND RECOMMENDATIONS

It has been shown that RAS almost perfectly simulates the experiment consisting of recording successive, regularly spaced wave elevation samples for a finite duration. In this respect, it is preferable to DAS, which unrealistically produces the same spectral moments at each realization.

More precisely, answers have been brought to the questions stressed at the end of [1] with regard to the probability law followed by the average power estimator and to the statistical relationships between discrete successive simulation points.

The signals generated with RAS and DAS are periodic. It has been shown that avoiding periodicity, by using fewer, nonharmonic frequency components, necessarily results in a deterioration of the statistical properties of the generated signal (with respect to the target sea state). Instead, if periodicity is an issue in the application considered, it is suggested to simply discard the initial or final k samples of the signals generated through RAS or DAS, where k is the number of lags beyond which the autocorrelation of the target spectrum is considered to be zero.

The consequences of the simulation method on time-domain statistics have been explored theoretically and experimentally.

With RAS (and in a true Gaussian sea) finite-length estimators for the wave signal energy, or for the WEC average power output, present a variance that is inversely proportional to the simulation length. Eventually, by running many simulations, or by increasing the simulation length, the value considered can be obtained with the desired accuracy. Furthermore, RAS exactly reflects how short-term WEC performance varies with respect to its long-term average, i.e., the value that would be obtained if the same Gaussian sea state were to last forever.

With DAS, only one simulation is necessary to obtain the average energy of the wave signal or, with a linear WEC, the average WEC power output. Even in a case where the WEC is weakly nonlinear, fewer simulations than with RAS, or equally a shorter simulation duration, are necessary to achieve the same degree of accuracy for the average WEC power estimate. However, DAS does not reproduce the variability of the short-term WEC performance in an actual sea. In addition, it might be possible that in some cases involving a strongly nonlinear WEC, DAS would result in biased power estimates. In contrast, regardless of the WEC model, it is certain that running WEC simulations based on RAS allows for unbiased estimates of the average WEC power output, and for realistic assessment of how the WEC power output may vary when measured over a finite duration.

Regarding more complex statistics related to individual oscillations of the signal ($H_{33\%}$, etc.), whether the signal is the wave itself or a WEC output such as position, velocity, or force, no analytical solutions can be easily derived for theoretical study. However, numerical experiments tend to show that while only a few simulations DAS results in statistics closer to long-term statistics, RAS shows how statistics may vary when estimated on a finite duration. As was already suggested in [1], covering the whole wave input probability space, by using several RAS-based simulations, could be especially important to study the device safety and survivability, considered with respect to a given sea state and a given time duration. In particular, DAS does not allow the observation of densities of big waves as high as RAS does.

In summary, by running several simulations with RAS, it can be ensured that the whole operational space of the device is covered with respect to a given sea spectrum and a finite time duration. Table II summarizes the main recommendations that can be provided in view of the results presented in this paper.

Finally, with respect to the computational burden of either DAS or RAS, in the unlikely case where time-series generation represents a significant fraction of the simulation time, two ideas are suggested to reduce their computational cost: replace large simulations by groups of shorter simulations, and combine FFT with spline interpolation to obtain generated points with a refined time resolution.

REFERENCES

[1] J.-B. Saulnier, P. Ricci, A. Clément, and A. D. O. Falcão, "Mean power output estimation of WECs in simulated sea," in *Proc. 8th Eur. Wave Tidal Energy Conf.*, Uppsala, Sweden, 2009, vol. 710, pp. 891–900.

[2] M. Tucker, P. Challenor, and D. Carter, "Numerical simulation of a random sea: A common error and its effect upon wave group statistics," *Appl. Ocean Res.*, vol. 6, no. 2, pp. 118–122, 1984. [Online]. Available: http://www.sciencedirect.com/science/article/pii/0141118784900506

[3] D. N. Veritas, "Modelling and analysis of marine operations," Det Norske Veritas, Oslo, Norway, Tech. Rep. DNV-RP-H103, 2011.

[4] M. K. Ochi, *Ocean Waves: The Stochastic Approach*, vol. 6. Cambridge, U.K., Cambridge Univ. Press, 2005.

[5] K. Hasselmann *et al.*, "Measurements of wind-wave growth and swell decay during the joint north sea wave project (JONSWAP)," Dtsch. Hydrogr. Inst., Hamburg, Germany, Tech. Rep., 1973.

[6] P. J. Brockwell and R. A. Davis, *Introduction to Time Series and Forecasting*. New York, NY, USA: Springer Science & Business Media, 2006.

[7] D. B. Percival, "Simulating Gaussian random processes with specified spectra," *Comput. Sci. Stat.*, vol. 24, pp. 534–534, 1993.

[8] J. Falnes, *Ocean Waves and Oscillating Systems: Linear Interactions Including Wave-energy Extraction*. Cambridge, U.K., Cambridge Univ. Press, 2002.

[9] J. Dale, "Estimation of the variance of a stationary Gaussian random process by periodic sampling," *Bell Syst. Tech. J.*, vol. 46, no. 6, pp. 1283–1287, 1967.

[10] A. V. Oppenheim and R. W. Schafer, *Discrete-Time Signal Processing*. London, U.K.: Pearson Higher Education, 2010.

[11] G. E. Box *et al.*, "Some theorems on quadratic forms applied in the study of analysis of variance problems, I. Effect of inequality of variance in the one-way classification," *Ann. Math. Stat.*, vol. 25, no. 2, pp. 290–302, 1954.

[12] E. Bækkedal, "Alternative methods of realizing the sea spectrum for time-domain simulations of marine structures in irregular seas," M.S. thesis, Dept. Marine Technol., Norwegian Univ. Sci. Technol., Trondheim, Norway, 2014.

[13] Y. Gōda, *Random Seas and Design of Maritime Structures (Advanced Series on Ocean Engineering)*. Singapore: World Scientific, 2000, vol. 15.

[14] V. Belenky, "Risk evaluation at extreme seas," in *Proc. 7th Int. Ship Stability Workshop*, Shanghai, China, 2004, pp. 188–202.

[15] C. Maisondieu, "WEC survivability threshold and extractable wave power," in *Proc. 11th Eur. Wave Tidal Energy Conf.*, 2015.

[16] H. Santo, P. Taylor, and R. Gibson, "Decadal variability of extreme wave height representing storm severity in the northeast Atlantic and north sea since the foundation of the royal society," *Proc. Roy. Soc. Amer.*, vol. 472, no. 2193, 2016, Art. no. 20160376.

[17] S. Ambühl, M. Kramer, J. P. Kofoed, J. D. Sørensen, and C. B. Ferreira, "Reliability assessment of wave energy devices," in *Safety, Reliability, Risk and Life-Cycle Performance of Structures and Infrastructures*. Boca Raton, FL, USA: CRC Press, 2014, pp. 5195–5202.

Alexis Mérigaud received the Engineering degree in 2012 from École Nationale Supérieure de Techniques (ENSTA ParisTech) Avancées, Palaiseau, France, where he specialized in energy management and economics. He then studied public administration for two years at Sciences Po, Paris, France. Since January 2015, he has been working toward the Ph.D. degree in the Centre for Ocean Energy Research, Maynooth University, Maynooth, Ireland.

He is currently working on energy forecasting and predictive maintenance applied to marine renewable energy sources. His previous experience in the field of energy includes economic modeling as well as technical regulatory aspects of energy networks and markets.

John V. Ringwood (M'87–SM'97) received the Diploma degree in electrical engineering from Dublin Institute of Technology, Dublin, Ireland, and the Ph.D. degree in control systems from Strathclyde University, Glasgow, U.K., in 1981 and 1985, respectively.

He is currently a Professor of Electronic Engineering and the Director of the Centre for Ocean Energy Research, Maynooth University, Maynooth, Ireland. He was the Head of the Electronic Engineering Department at NUI Maynooth from 2000 to 2005, developing the department from a greenfield site. His research interests cover time-series modeling, wave energy, control of plasma processes, and biomedical engineering.

Dr. Ringwood is a Chartered Engineer and a Fellow of the Institution of Engineers of Ireland.